Inorganic Chemistry
Article

Inorg. Chem. **2009**, *48*, 8233–8244 **8233**
DOI: 10.1021/ic9008043

Soluble Redox-Active Polymetallic Chains $[\{Ru^0(CO)(L)(bpy)\}^m]_n$ (bpy = 2,2′-bipyridine, L = PrCN, Cl^-; $m = 0, -1$): Electrosynthesis and Characterization

František Hartl,*,† Anna K. Renfrew,‡ Frédéric Lafolet,‡ Taasje Mahabiersing,§ Maria José Calhorda,∥ Sylvie Chardon-Noblat,*,‡ Matti Haukka,⊥ and Alain Deronzier‡

†*Department of Chemistry, University of Reading, Whiteknights, Reading, RG6 6AD, United Kingdom,* ‡*Université Joseph Fourier Grenoble 1, Département de Chimie Moléculaire, UMR CNRS-5250, Institut de Chimie Moléculaire de Grenoble FR CNRS-2607, B.P. 53, 38041 Grenoble Cedex 9, France,* §*Van't Hoff Institute for Molecular Sciences, University of Amsterdam, Nieuwe Achtergracht 166, 1018 WV Amsterdam, The Netherlands,* ∥*Departamento de Química e Bioquímica, CQB, Faculdade de Ciências, Universidade de Lisboa, Campo Grande, 1749-016 Lisboa, Portugal, and* ⊥*Department of Chemistry, University of Joensuu, P.O. Box 111, 80101 Joensuu, Finland*

Received April 25, 2009

Electrochemical and spectroelectrochemical techniques were employed to study in detail the formation and so far unreported spectroscopic properties of soluble electroactive molecular chains with nonbridged metal−metal backbones, namely, $[\{Ru^0(CO)(PrCN)(bpy)\}^m]_n$ ($m = 0, -1$) and $[\{Ru^0(CO)(bpy)Cl\}^m]_n$ ($m = -1, -2$; bpy = 2,2′-bipyridine). The precursors *cis*-(Cl)-$[Ru^{II}(CO)(MeCN)(bpy)Cl_2]$ (in PrCN) and *mer*-$[Ru^{II}(CO)(bpy)Cl_3]^-$ (in tetrahydrofuran (THF) and PrCN) undergo one-electron reductions to reactive radicals $[Ru^{II}(CO)(MeCN)(bpy^{\bullet-})Cl_2]^-$ and $[Ru^{II}(CO)(bpy^{\bullet-})Cl_3]^{2-}$, respectively. Both $[bpy^{\bullet-}]$-containing species readily electropolymerize on concomitant dissociation of two chloride ligands and consumption of a second electron. Along this path, mer-to-fac isomerization of the bpy-reduced trichlorido complex (supported by density functional theory calculations) and a concentration-dependent oligomerization process contribute to the complex reactivity pattern. In situ spectroelectrochemistry (IR, UV/vis) has revealed that the charged polymer $[\{Ru^0(CO)(bpy)Cl\}^-]_n$ is stable in THF, but in PrCN it converts readily to $[Ru^0(CO)(PrCN)(bpy)]_n$. An excess of chloride ions retards this substitution at low temperatures. Both polymetallic chains are completely soluble in the electrolyte solution and can be reduced reversibly to the corresponding $[bpy^{\bullet-}]$-containing species.

Introduction

Examples of polymeric complexes consisting of unsupported metal−metal-bonded linear chains are rather rare in the literature. The priority belongs to the simple $[Ru^0(CO)_4]_n$ polymer reported in 1986 by Hastings and Baird.[1] Its structure was characterized by Masciocchi et al.[2] and more recently examined by Hirva et al. using density functional theory (DFT).[3] The unusual binary complex $\{[Rh(MeCN)_4](BF_4)_{1.5}\}_n$ (MeCN = acetonitrile) containing a mixed-valence rhodium backbone has been known since the mid-1990s.[4] Polymetallic compounds belonging to this class are believed to find application as conducting molecular wires in the expanding field of molecular electronics and nanoscale molecular devices.[5] More recently, several related complexes, $\{[Rh_2(NN)_2(\mu\text{-}O_2CMe)_2](BX_4)\}_n$ (NN = 2,2′-bipyridine (bpy) or 1,10-phenanthroline; X = F, Ph), have been prepared and characterized by Pruchnik et al.,[6,7] some of them exhibiting interesting redox behavior.[8,9]

*To whom correspondence should be addressed. E-mail: f.hartl@reading.ac.uk, f.hartl@uva.nl (F.H.).

(1) Hastings, W. R.; Baird, M. C. *Inorg. Chem.* **1986**, *25*, 2913–2915.
(2) Masciocchi, N.; Moret, M.; Cairati, P.; Ragaini, F.; Sironi, A. *J. Chem. Soc., Dalton Trans.* **1993**, 471–475.
(3) Niskanen, M.; Hirva, P.; Haukka, M. *J. Chem. Theor. Comput.* **2009**, *5*, 1084–1090.
(4) (a) Finniss, G. M.; Canadell, M.; Campana, C.; Dunbar, K. R. *Angew. Chem., Int. Ed. Engl.* **1996**, *35*, 2772–2774. (b) Prater, M. E.; Pence, L. E.; Clérac, R.; Finniss, G. M.; Campana, C.; Auban-Senzier, P.; Jérome, D.; Canadell, E.; Dunbar, K. R. *J. Am. Chem. Soc.* **1999**, *121*, 8005–8016. (c) Bera, J. K.; Dunbar, K. R. *Angew. Chem., Int. Ed.* **2002**, *41*, 4453–4457.
(5) Tyler, D. R. *Frontiers in Transition Metal-Containing Polymers*; Abd-El-Aziz, S. A., Manners, I., Eds.; Wiley-Interscience: Weinheim, Germany, 2007; p 287.
(6) (a) Pruchnik, F. P.; Jakimowicz, P.; Ciunik, Z. *Inorg. Chem. Commun.* **2001**, *4*, 19–22. (b) Pruchnik, F. P.; Jakimowicz, P.; Ciunik, Z.; Stanislawek, K.; Oro, L. A.; Tejel, C.; Ciriano, M. A. *Inorg. Chem. Commun.* **2001**, *4*, 726–729.
(7) (a) Pruchnik, F. P.; Jutarska, A.; Ciunik, Z.; Pruchnik, M. *Inorg. Chim. Acta* **2003**, *350*, 609–616. (b) Pruchnik, F. P.; Jutarska, A.; Ciunik, Z.; Pruchnik, M. *Inorg. Chim. Acta* **2004**, *357*, 3019–3026.
(8) Lafolet, F.; Chardon-Noblat, S.; Duboc, C.; Deronzier, A.; Pruchnik, F. P.; Rak, M. *Dalton Trans.* **2008**, 2149–2156.
(9) Rak, M.; Pruchnik, F. P.; Ciunik, L. Z.; Lafolet, F.; Chardon-Noblat, S.; Deronzier, A. *Eur. J. Inorg. Chem.* **2009**, 111–118.

Published on Web 08/05/2009

Another important type of redox-active metal−metal-bonded chain complex, $[Ru(CO)_2(bpy)]_n$, has been known for more than 15 years as an excellent catalyst of the water-gas shift reaction (WGSR) and the currently highly topical electrochemical reduction of carbon dioxide in aqueous media.[10] It operates at moderate overpotentials in aqueous media, and the product selectivity toward $CO/HCOO^-$ can be tuned by varying substituents at the bpy ligands.[11] $[Ru(CO)_2(bpy)]_n$ can be prepared straightforwardly by a two-electron-consuming electropolymerization of the mononuclear dichlorido or bis(acetonitrile) Ru(II) dicarbonyls on conductive surfaces as strongly adherent thin films. The intimate mechanism of the electropolymerization has been fairly well understood, involving the formation of dimeric, tetrameric, and higher oligomeric intermediates along the electrochemical propagation path (see for instance eqs 1−3). This is a consequence of easier or similar reducibility of the intermediate oligomeric complexes.[12]

$$[Ru^{II}(CO)_2(bpy)Cl_2] + e^- \rightarrow [Ru^{II}(CO)_2(bpy^{\bullet -})Cl_2]^- \quad (1)$$

$$[Ru^{II}(CO)_2(bpy^{\bullet -})Cl_2]^- \rightarrow 1/2[Ru^{I}(CO)_2(bpy)Cl]_2 + Cl^- \quad (2)$$

$$n/2[Ru^{I}(CO)_2(bpy)Cl]_2 + ne^- \rightarrow \rightarrow [Ru^0(CO)_2(bpy)]_n + nCl^- \quad (3)$$

The poor solubility of polymeric $[Ru(CO)_2(bpy)]_n$, however, limits its utilization as an active catalyst. For example, it is difficult to disperse it onto supports like SiO_2 for catalytic WGSR applications.[13] The more practical way to achieve this goal is to electrodeposit the polymer directly onto a conductive support material. We have therefore attempted to prepare and characterize soluble representatives of this linear polymeric catalyst. The first literature report dealt with electropolymerization of *mer*-$[Ru^{II}(CO)(bpy)Cl_3]^-$ (Chart 1) in acetonitrile. Two-electron reduction of this complex led to a largely soluble product that was never fully characterized.[14,15] However, it was shown to form very thin films at the working-electrode surface upon prolonged exhaustive reduction at a controlled potential in acetonitrile containing 5% H_2O. The resulting redox-active film proved to be a good electrocatalyst converting CO_2 quantitatively into CO.[15] Another suitable candidate for the preparation of soluble polymers is the complex *cis*-(Cl)-$[Ru^{II}(CO)(MeCN)(bpy)Cl_2]$ (Chart 1), originally synthesized from the dichlorido dicarbonyl precursor by selective photosubstitution in MeCN (eq 4).[16]

Chart 1. Schematic Representation of the Investigated Complexes *cis*-(Cl)-$[Ru^{II}(CO)(MeCN)(bpy)Cl_2]$ and *mer*-$[Ru^{II}(CO)(bpy)Cl_3]^-$ and the Corresponding Two-Electron-Reduced Ru(0) Polymer Chains

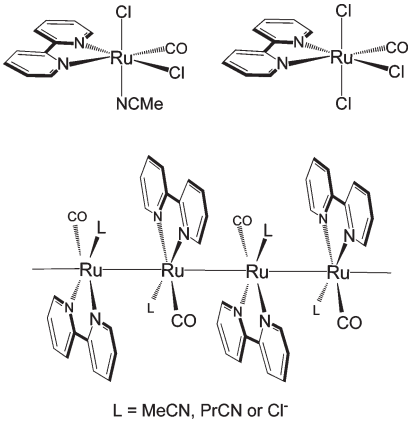

$$[Ru(CO)_2(bpy)Cl_2] + MeCN \xrightarrow{h\nu} [Ru(CO)(MeCN)(bpy)Cl_2] + CO \quad (4)$$

The redox behavior of *cis*-(Cl)-$[Ru^{II}(CO)(MeCN)(bpy)Cl_2]$ was studied only marginally. It turned out, however, that its exhaustive reduction in acetonitrile led to a soluble species, which was not further characterized.[17]

The big difference in solubility between dicarbonyl and monocarbonyl polymeric chains in acetonitrile has recently been documented for closely related osmium(0) species $[Os(CO)_2(bpy)]_n$ (poorly soluble, forming films and a voluminous precipitate) and $[Os(CO)(MeCN)(bpy)]_n$ (completely soluble).[18,19] It is noteworthy that the solubility of the dicarbonyl polymeric species strongly increases in butyronitrile, which is therefore a more convenient solvent for conducting their spectroelectrochemical studies.

Given the incomplete information in the literature, the major goal of this work was a detailed voltammetric and spectroelectrochemical investigation of the two-electron reduction paths of *cis*-(Cl)-$[Ru^{II}(CO)(MeCN)(bpy)Cl_2]$ and *mer*-$[Ru^{II}(CO)(bpy)Cl_3]^-$ (Chart 1) in different solvents (acetonitrile, butyronitrile, and tetrahydrofuran (THF)). Special attention was paid to the characterization of the postulated soluble metal−metal-bonded polymer products (Chart 1).

Experimental Section

Materials and Preparations. CO gas (99%) was purchased from AGA. All solvents were of analytical grade. Methanol (MeOH; 99.8%, J. T. Baker) was used directly for synthesis. THF, MeCN, and butyronitrile (PrCN) for spectroelectrochemical measurements (all Acros Chimica) were dried by standard procedures[20] and freshly distilled under dry nitrogen prior to

(10) Chardon-Noblat, S.; Deronzier, A.; Ziessel, R. *Collect. Czech. Chem. Commun.* **2001**, *66*, 207−227, and references therein.
(11) Chardon-Noblat, S.; Deronzier, A.; Ziessel, R.; Zsoldos, D. *J. Electroanal. Chem.* **1998**, *444*, 253–260.
(12) Chardon-Noblat, S.; Deronzier, A.; Zsoldos, D.; Ziessel, R.; Haukka, M.; Pakkanen, T. A.; Venäläinen, T. *J. Chem. Soc., Dalton Trans.* **1996**, 2581–2583.
(13) Luukkanen, S.; Homanen, P.; Haukka, M.; Pakkanen, T. A.; Deronzier, A.; Chardon-Noblat, S.; Zsoldos, D.; Ziessel, R. *Appl. Catal., A* **1999**, *185*, 157–164.
(14) Collomb-Dunand-Sauthier, M.-N.; Deronzier, A.; Ziessel, R. *J. Electroanal. Chem.* **1993**, *350*, 43–55.
(15) Collomb-Dunand-Sauthier, M.-N.; Deronzier, A.; Ziessel, R. *Inorg. Chem.* **1994**, *33*, 2961–2967.
(16) Eskelinen, E.; Haukka, M.; Venäläinen, T.; Pakkanen, T. A.; Wasberg, M.; Chardon-Noblat, S.; Deronzier, A. *Organometallics* **2000**, *19*, 163–169.
(17) Collomb-Dunand-Sauthier, M.-N.; Deronzier, A.; Ziessel, R. *J. Organomet. Chem.* **1993**, *444*, 191–198.
(18) Chardon-Noblat, S.; Deronzier, A.; Hartl, F.; van Slageren, J.; Mahabiersing, T. *Eur. J. Inorg. Chem.* **2001**, 613–617.
(19) Hartl, F.; Mahabiersing, T.; Chardon-Noblat, S.; Da Costa, P.; Deronzier, A. *Inorg. Chem.* **2004**, *43*, 7250–7258.
(20) Perrin, D. D.; Armarego, W. L. F. *Purification of Laboratory Chemicals*, 3rd ed.; Pergamon: Exeter, U.K., 1988.

use. The supporting electrolyte Bu_4NPF_6 (TBAH, Aldrich) was recrystallized twice from absolute ethanol (Acros Chimica) and dried at 80 °C for 3 days. Bu_4NClO_4 (TBAP) and Et_4NCl (TEACl; Fluka) were used without purification. Elemental analyses (C, N, H) were conducted on a CE Instruments EA 110 CHNS-O analyzer. All measurements were performed under an atmosphere of dry nitrogen or argon. Samples were prepared and handled by standard Schlenk techniques.

The complexes *trans*-(Cl)-[$Ru^{II}(CO)_2(bpy)Cl_2$] and *mer*-[Ru(MeOH)(bpy)Cl_3] were synthesized according to literature procedures.[21,22] The investigated reference complex *cis*-(Cl)-[Ru(CO)(MeCN)(bpy)Cl_2] was prepared from *trans*-(Cl)-[Ru$(CO)_2$(bpy)Cl_2] by a photochemical procedure described in the literature.[16] FTIR (acetonitrile): ν(CO) = 1968(vs) cm^{-1}. UV/vis (acetonitrile): λ_{max} = 450 nm.

***mer*-[Ru^{III}(CO)(bpy)Cl_3].** A sample of *mer*-[Ru(MeOH)(bpy)Cl_3] (100 mg, 0.255 mmol) and dichloromethane (20 mL) were heated in a 60 mL Berghof autoclave to 60 °C under 10 bar of CO pressure. The temperature was maintained at 60 °C for 18 h and then slowly reduced to 20 °C. The product was filtered off as a red powder, washed with a small amount of MeOH, and dried under a vacuum. Yield: 76%. FTIR (dichloromethane): ν(CO) = 2064(vs) cm^{-1}. UV/vis: see the main text (Figure 5A). Elem anal. calcd (%) for $C_{11}H_8OCl_3Ru$ (391.63): C, 33.73; H, 2.05; N, 7.15. Found: C, 33.70; H, 2.11; N, 7.16.

Instrumentation. Spectroscopy and Analysis. Infrared spectra for characterization purposes were recorded on Nicolet Magna 750 or Perkin-Elmer Spectrum GX FTIR spectrometers. The elemental analysis was carried out with a CE Instruments EA 110 CHNS-O setup.

Electrochemistry. Cyclic voltammograms were recorded in Amsterdam (A) and Grenoble (G) with an EG&G PAR model 283 potentiostat operated with the PAR Power CV software (A) and an EG&G PAR model 173 linked to a Sefram TGM 164 x-y recorder (G). The conventional airtight electrochemical cells contained the following electrode sets: (A) a 0.42 mm^2 microdisc working electrode polished between scans with a 0.25 μm diamond paste (Oberflächentechnologien Ziesmer, Kempen, Germany) placed in a (thermostatted) single compartment with a Pt wire auxiliary electrode and a Ag wire pseudoreference electrode (combined with the ferrocene/ferrocenium (Fc/Fc^+) redox couple used as an internal reference; (G) a 0.19 mm^2 Pt microdisc working electrode polished with a 2 μm diamond paste (Mecaprex Pressi), a Pt wire auxiliary electrode in MeCN/10^{-1} M Bu_4NPF_6 separated by a frit from the bulk solution, and a Ag/Ag^+ (10^{-2} M in acetonitrile/10^{-1} M Bu_4NPF_6) reference electrode. All electrode potentials reported here are relative to the Ag/Ag^+ reference electrode and can be converted to the standard[23] Fc/Fc^+ potential scale (in MeCN and PrCN) by adding −0.087 V to the measured value.[24] In THF, we recommend the use of a factor of −0.22 V, determined in this work by using ferrocene, cobaltocenium hexafluorophosphate (−1.33 V vs ferrocene), and acetylferrocene (+0.22 V vs ferrocene) as standards. Bulk electrolyses with the EG&G PAR model 173 potentiostat equipped with a digital coulometer (G) were carried out in a drybox (Jaram) on a Pt sheet (2 cm^2) placed on the cell together with the analytical Pt microdisc working electrode. The electrolyses were interrupted after the predetermined number of coulombs had passed and conventional cyclic voltammograms were subsequently recorded. The electrochemical samples were 1−3 mM in the studied complexes and 10^{-1} M in the supporting electrolyte.

Spectroelectrochemistry. UV/vis spectroelectrochemical experiments coupled to bulk electrolyses in a drybox (G) were performed using a Carl Zeiss MCS 501 UV-NIR diode spectrophotometer. The light sources were halogen CLH 500 20 W and deuterium CLD 500 lamps with a 041.002-UV SN 012105 optical fiber or using an additional 1 mm quartz immersion probe (Hellma). Thin-layer UV/vis and IR spectroelectrochemistry at laboratory and low temperatures (A) was carried out with optically transparent electrochemical (OTTLE) cells[25−27] equipped with Pt minigrid working and auxiliary electrodes, a Ag microwire pseudoreference electrode, and CaF_2 windows. Thin-layer cyclic voltammograms were recorded in the course of each OTTLE experiment for a precise potential control achieved with a PA4 potentiostat (EKOM, Polná, Czech Republic) and for monitoring of the progress of the electrolyses by decreasing the faradaic current. The spectroelectrochemical samples were typically 10^{-3} M (UV/vis) and 3×10^{-3} M (IR) in the studied complex and 3×10^{-1} M in the supporting electrolyte. UV/vis spectra of the electrolyzed solutions were obtained with a HP 8453 diode array spectrophotometer and IR spectra with a Bruker Vertex 70 FTIR spectrometer equipped with a DTGS detector (spectral resolution of 1 cm^{-1}) or connected to a cooled MCT detector (originally part of a Bio-Rad FTS-60A FTIR setup; spectral resolution of 2 cm^{-1}) for low-temperature spectroelectrochemistry.

Computational Work. DFT calculations[28] were performed using the Amsterdam Density Functional program package (ADF).[29] Gradient-corrected geometry optimizations[30] (gas-phase and solvent) were performed without symmetry constraints using the local density approximation of the correlation energy (Vosko−Wilk−Nusair)[31] augmented by the exchange-correlation functional of Becke and Perdew (BP86)[32] Triple-ζ Slater-type orbitals were used to describe the valence shells of N, C, O, H, and Ru, with a set of two polarization functions (p,f for Ru; d,f for Cl, N, C, O; and p,d for H). The core orbitals were frozen for Ru ([1−3]s, [2−3]p, [3]d), Cl ([1−2]s, 2p), N, C, and O (1s). The relativistic effects were treated with the ZORA approximation.[33] Time-dependent DFT (TD-DFT) calculations were performed to determine electronic transitions.[34] The solvent effects were included using the COnductor-like Screening MOdel (COSMO)[35] implemented in ADF. The rigid

(21) Chardon-Noblat, S.; Deronzier, A.; Ziessel, R.; Zsoldos, D. *Inorg. Chem.* **1997**, *36*, 5384–5389.
(22) Eskelinen, E.; Da Costa, P.; Haukka, M. *J. Electroanal. Chem.* **2005**, *579*, 257–265.
(23) Gritzner, G.; Kůta, J. *Pure Appl. Chem.* **1984**, *56*, 461–466.
(24) Pavlishchuk, V. V.; Addison, A. W. *Inorg. Chim. Acta* **2000**, *298*, 97–102.
(25) Hartl, F.; Luyten, H.; Nieuwenhuis, H. A.; Schoemaker, G. C. *Appl. Spectrosc.* **1994**, *48*, 1522–1528.
(26) Mahabiersing, T.; Luyten, H.; Nieuwendam, R. C.; Hartl, F. *Collect. Czech. Chem. Commun.* **2003**, *68*, 1687–1709.
(27) Krejčík, M.; Daněk, M.; Hartl, F. *J. Electroanal. Chem. Interfacial Electrochem.* **1991**, *317*, 179–187.
(28) Parr, R. G.; Yang, W. *Density Functional Theory of Atoms and Molecules*; Oxford University Press: New York, 1989.
(29) (a) te Velde, G.; Bickelhaupt, F. M.; van Gisbergen, S. J. A.; Guerra, C. F.; Baerends, E. J.; Snijders, J. G.; Ziegler, T. *J. Comput. Chem.* **2001**, *22*, 931–967. (b) Guerra, C. F.; Snijders, J. G.; te Velde, G.; Baerends, E. J. *Theor. Chem. Acc.* **1998**, *99*, 391–403. (c) *ADF2007*; SCM, Theoretical Chemistry, Vrije Universiteit: Amsterdam, The Netherlands. http://www.scm.com (accessed July 2009).
(30) (a) Versluis, L.; Ziegler, T. *J. Chem. Phys.* **1988**, *88*, 322–328. (b) Fan, L.; Ziegler, T. *J. Chem. Phys.* **1991**, *95*, 7401–7408.
(31) Vosko, S. H.; Wilk, L.; Nusair, M. *Can. J. Phys.* **1980**, *58*, 1200–1211.
(32) (a) Becke, A. D. *J. Chem. Phys.* **1987**, *88*, 1053–1062. (b) Perdew, J. P. *Phys. Rev.* **1986**, *B33*, 8822–8824. (c) Perdew, J. P. *Phys. Rev.* **1986**, *B34*, 7406.
(33) van Lenthe, E.; Ehlers, A.; Baerends, E. J. *J. Chem. Phys.* **1999**, *110*, 8943–8953.
(34) (a) van Gisbergen, S. J. A.; Groeneveld, J. A.; Rosa, A.; Snijders, J. G.; Baerends, E. J. *J. Phys. Chem.* **1999**, *103A*, 6835–6844. (b) Rosa, A.; Baerends, E. J.; van Gisbergen, S. J. A.; van Lenthe, E.; Groeneveld, J. A.; Snijders, J. G. *J. Am. Chem. Soc.* **1999**, *121*, 10356–10365. (c) van Gisbergen, S. J. A.; Rosa, A.; Ricciardi, G.; Baerends, E. J. *J. Chem. Phys.* **1999**, *111*, 2499–2506.
(35) (a) Klamt, A.; Schürmann, G. *J. Chem. Soc., Perkin Trans. 2* **1993**, 799–805. (b) Klamt, A. *J. Phys. Chem.* **1995**, *99*, 2224–2235. (c) Klamt, A.; Jones, V. *J. Chem. Phys.* **1996**, *105*, 9972–9981. (c) Pye, C. C.; Ziegler, T. *Theor. Chem. Acc.* **1999**, *101*, 396–408.

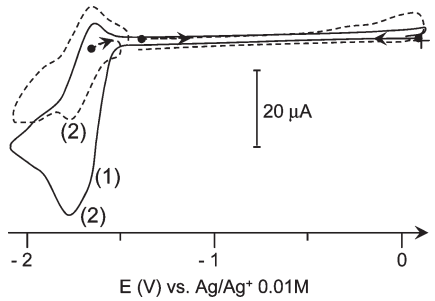

Figure 1. CVs at a vitreous carbon electrode (3 mm diameter). Solid curve: *cis*-(Cl)-[Ru(CO)(MeCN)(bpy)Cl_2] (2.2 mM in PrCN containing 0.1 M TBAP), initial scan. Dashed curve: $[Ru(CO)(PrCN)(bpy)]_n$ after exhaustive two-electron reduction of the dichloride complex at −1.81 V. Scan rate = 100 mV s^{-1}, T = 293 K.

sphere radius of the THF solvent molecules was taken to be 3.18 Å,[36] and the dielectric constant was 7.58. The van der Waals radii of the atoms were used for the atomic radius of the solute (or atomic radius in the case of Ru): Ru, 134 pm; Cl, 175 pm; N, 155 pm; C, 170 pm; O, 152 pm; H, 120 pm.[37] Mayer bond orders[38] were calculated as implemented in ADF.

Results and Discussion

Redox Properties and Cathodic Polymerization of *cis*-(Cl)-[Ru^{II}(CO)(MeCN)(bpy)Cl_2]. Cyclic Voltammetry. The cyclic voltammogram (CV) of the complex in MeCN or PrCN shows a reversible anodic wave at $E_{1/2}$ = +0.76 V, which corresponds formally to the Ru(II)/Ru(III) couple. This value is more positive by 0.31 V than the oxidation potential of the corresponding Os(II) complex. A slightly smaller difference was observed for the more positively oxidized complexes [$M(CO)_2$(bpy)Cl_2], M = Ru and Os, where $\Delta E_{1/2}$ = 0.22 V.[18]

In the cathodic region, the complex *cis*-(Cl)-[Ru(CO)(MeCN)(bpy)Cl_2] in PrCN undergoes at room temperature (RT) a chemically totally irreversible reduction at $E_{p,c}$ = −1.78 V, followed by an apparently reversible redox couple at $E_{1/2}$ = −1.84 V (Figure 1). A similar CV scan in MeCN was previously reported in the literature.[17]

Bulk electrolysis of *cis*-(Cl)-[Ru(CO)(MeCN)(bpy)Cl_2] at −1.81 V in PrCN yielded after consumption of two electrons a soluble species reversibly reducible at $E_{1/2}$ = −1.84 V (redox couple 2 in Figure 1, dashed line). The cathodic process corresponds to polymerization described by eq 5, which was confirmed by the corresponding spectroelectrochemical study.

$$n[Ru^{II}(CO)(MeCN)(bpy)Cl_2] + 2ne^- + n\text{PrCN} \rightarrow [Ru^0(CO)(PrCN)(bpy)]_n + 2nCl^- + n\text{MeCN} \quad (5)$$

The reversible cathodic response of the polymer $[Ru^0(CO)(PrCN)(bpy)]_n$ (Chart 1) at $E_{1/2}$ = −1.84 V (ΔE_p = 150 mV) is characteristic for this class of chain compounds, corresponding to the one-electron reduction of the bpy ligands (eq 6).

$$[Ru^0(CO)(PrCN)(bpy)]_n + ne^- \rightarrow [\{Ru^0(CO)(PrCN)(bpy^{\bullet -})\}^-]_n \quad (6)$$

In contrast, the cyclic voltammogram of *cis*-(Cl)-[Ru(CO)(MeCN)(bpy)Cl_2] recorded at a low temperature (213 K) in PrCN containing an excess of the Et_4NCl electrolyte showed a fully reversible single cathodic response at $E_{1/2}$ = −1.84 V (ΔE_p = 70 mV). Warming up the electrolyte to room temperature made this cathodic process irreversible and gradually shifted it back to $E_{p,c}$ = −1.78 V, with the concomitant growth of the slightly more negative polymer response (cf. Figure 1). This behavior reflects the stability of one-electron-reduced [Ru^{II}(CO)(RCN)(bpy$^{\bullet -}$)Cl_2]$^-$ (R = Me or Pr) achieved at sufficiently low temperatures in the presence of the chloride anions (eq 7).

$$[Ru^{II}(CO)(RCN)(bpy)Cl_2] + 1e^- \rightarrow [Ru^{II}(CO)(RCN)(bpy^{\bullet -})Cl_2]^- \quad (7)$$

At RT, the bpy-reduced radical species is very reactive, expelling both chlorido ligands and converting to the polymeric Ru^0-bpy compound (eq 8), as evidenced by spectroelectrochemistry (see below).

$$n[Ru^{II}(CO)(RCN)(bpy^{\bullet -})Cl_2]^- + ne^- \rightarrow [Ru^0(CO)(RCN)(bpy)]_n + 2nCl^- \quad (8)$$

It is noteworthy that the bpy ligands in [Ru^0(CO)(RCN)(bpy)]$_n$ (293 K) and parent *cis*-(Cl)-[Ru^{II}(CO)(RCN)(bpy)Cl_2] (213 K) are reduced at the same electrode potential. For comparison, the closely related polymer $[Os^0(CO)(MeCN)(bpy)]_n$ undergoes the reversible bpy-localized reduction at $E_{1/2}$ = −2.06 V, that is, at a much lower potential ($\Delta E_{1/2}$ = 270 mV) than the parent mononuclear complex *trans*-(Cl)-[Os^{II}(CO)(MeCN)(bpy)Cl_2] ($E_{1/2}$ = −1.79 V).[19] This variation of the bpy-reduction potentials reflects the different geometries of the M(II) dichlorido complexes.[39]

Spectroelectrochemistry. Electrochemical reduction of *cis*-(Cl)-[Ru^{II}(CO)(MeCN)(bpy)Cl_2] in PrCN at RT was monitored in situ by IR and UV/vis spectroscopies, using an OTTLE cell. It has been documented that redox and spectroscopic properties of related carbonyl complexes containing PrCN and MeCN ligands are almost identical.[40] In this case,

(36) Reid, R. C.; Prausnitz, J. M.; Poling, B. E. *The Properties of Gases and Liquids*, 4th ed.; McGraw-Hill International: New York, 1987; Appendix B, pp 733−734.
(37) Bondi, A. *J. Phys. Chem.* **1964**, *68*, 441–451.
(38) Mayer, I. *Int. J. Quantum Chem.* **1986**, *29*, 73–84.

(39) Os complexes are reduced typically more negatively than their Ru counterparts, namely, [Ru(CO)(MeCN)(bpy)]$_n$ ($E_{1/2}$ = −1.84 V) versus [Os(CO)(MeCN)(bpy)]$_n$ ($E_{1/2}$ = −2.06 V) and *trans*-(Cl)-[Ru(CO)$_2$(bpy)Cl_2] ($E_{p,c}$ = −1.50 V) versus *trans*-(Cl)-[Os(CO)$_2$(bpy)Cl_2] ($E_{p,c}$ = −1.61 V). The hypothetical isomer *trans*-(Cl)-[Ru^{II}(CO)(MeCN)(bpy)Cl_2] is likely to have a less negative reduction potential than the investigated *cis*-(Cl) isomer, due to less donating axial chlorido ligands. This assumption is supported by the fact that the *trans*-(Cl)-[Os^{II}(CO)(MeCN)(bpy)Cl_2] and *cis*-(Cl)-[Ru^{II}(CO)(MeCN)(bpy)Cl_2] complexes have almost identical reduction potentials. For comparison, *cis*-(Cl)-[Ru(CO)$_2$(bpy)Cl_2] ($E_{p,c}$ = −1.54 V) also reduces more negatively than *trans*-(Cl)-[Ru(CO)$_2$(bpy)Cl_2] ($E_{p,c}$ = −1.50 V); a larger potential difference (>100 mV) is expected for the reduction of the corresponding MeCN-substituted monocarbonyl complexes.
(40) Johnson, F. P. A.; George, M. W.; Hartl, F.; Turner, J. J. *Organometallics* **1996**, *15*, 3374–3387. Compare the reduction potentials and CO-stretching frequencies of the complexes *fac*-[Re(CO)$_3$(L)(bpy)]^m (L = MeCN, PrCN; m = +1, 0, −1).

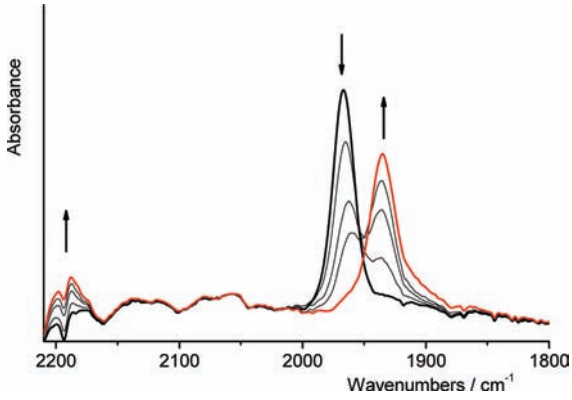

Figure 2. Infrared spectral changes accompanying the reduction of *cis*-(Cl)-[Ru(CO)(MeCN)(bpy)Cl_2] to [Ru(CO)(PrCN)(bpy)]$_n$ in PrCN/TBAH at T = 293 K, recorded using an OTTLE cell.

we may reasonably assume[41] that the bulk PrCN solvent replaced completely the MeCN ligand in the course of the electrolysis (eq 5).

Passing carefully the irreversible cathodic peak at −1.78 V resulted in a gradual shift of the strong CO-stretching band at 1967 cm^{-1} to 1935 cm^{-1} ($\Delta\nu$ = −32 cm^{-1} ; Figure 2). At the same time, a new band of low/medium intensity grew up at 2194 cm^{-1}. This absorption signature has been assigned to the C≡N stretch of the PrCN ligand coordinated at the electron-rich Ru(0) center. The significant ν(C≡N) shift ($\Delta\nu$ = −80 cm^{-1}) from 2274 cm^{-1} in the *cis*-(Cl)-[Ru(CO)(MeCN)(bpy)Cl_2] parent complex[17] agrees with the presence of the PrCN ligand in the two-electron-reduced polymer [Ru(CO)(PrCN)(bpy)]$_n$ (eq 5), reflecting its involvement in the stabilizing π-back-donation from the Ru(0) center.[42]

The cathodic polymerization of the complex *cis*-(Cl)-[Ru(CO)(MeCN)(bpy)Cl_2] in PrCN (eq 5) was also monitored in situ by UV/vis spectroscopy. The characteristic (Ru−Cl)-to-bpy (M−X)LCT absorption band of the parent complex at 465 nm (see Figure SI3 in Supporting Information)[43−45] was replaced on retention of isosbestic points by a new, comparably intense absorption band of [Ru^0(CO)(PrCN)(bpy)]$_n$, at 386 nm with a shoulder at 415 nm, accompanied by a broad and weak absorption centered at 560 nm (identical to the product spectrum in Figure 5B, see below).

Ultimate evidence for the formation of the polymer [Ru(CO)(PrCN)(bpy)]$_n$ was obtained from potential-controlled coulometry of *cis*-(Cl)-[Ru(CO)(MeCN)(bpy)Cl_2] in PrCN on a Pt sheet electrode. Exhaustive reduction of the parent complex at −1.80 V with two electrons gave the same, completely soluble product as observed with IR and UV/vis spectroelectrochemistry (see above). This result is consistent with dissociation of the two Cl^- ligands in the parent complex required for growing the polymeric chain.

The CO and PrCN ligands in [Ru(CO)(PrCN)(bpy)]$_n$ were thus identified by IR spectroscopy, and the presence of the neutral bpy ligand was revealed by the reduction of the polymer in the next step at the reversible cathodic wave at −1.84 V (the redox system (2) in Figure 1). UV/vis spectroelectrochemistry showed smooth isosbestic conversion of the starting polymer to its one-electron-reduced form [{Ru^0(CO)(PrCN)(bpy$^{\bullet-}$)}$^-$]$_n$ (eq 6). The presence of the reduced [bpy$^{\bullet-}$] ligand in the product was clearly manifested by its typical intraligand absorption,[19] namely, a bifurcated $\pi^*\pi^*$ absorption band at 502 and 532 nm accompanied by a new intense $\pi\pi^*$ band at 387 nm and a weak $\pi^*\pi^*$ absorption below 800 nm (Figure 5C). In the IR spectra, the bpy-localized $1e^-$ reduction is consistent with the small wavenumber shifts of the ν(C≡O) band from 1935 cm^{-1} to 1910 cm^{-1} and of the butyronitrile ν(C≡N) band from 2194 cm^{-1} to 2183 cm^{-1} (Figure 3). These spectral changes were fully reversible.

The reduction of *cis*-(Cl)-[Ru(CO)(MeCN)(bpy)Cl_2] (ν(C≡O) at 1968 cm^{-1}) in a thin layer of THF, monitored by IR spectroscopy, produced exclusively [Ru(CO)(MeCN)(bpy)]$_n$ (ν(C≡O) at 1934 cm^{-1}) that was further reducible to less-soluble [{Ru^0(CO)(MeCN)(bpy$^{\bullet-}$)}$^-$]$_n$ (ν(C≡O) at 1910 cm^{-1}). It is worth mentioning that the ν(C≡O) band of the latter negatively charged polymer species is markedly broader in THF than observed under the same conditions in more polar PrCN (Figure 3). These results confirm that the nitrile ligands are firmly bound at the metallic polymer backbone.

Cathodic Polymerization of *mer*-[Ru(CO)(bpy)Cl_3]$^-$ in PrCN. Cyclic Voltammetry. The complex *mer*-[Ru(CO)(bpy)Cl_3] (Chart 1) is reduced in PrCN at $E_{1/2}$ = +0.16 V (RT) to the corresponding Ru(II) anionic product in a fully reversible step (eq 9). The reversibility of the Ru(II)/Ru(III) couple reflects preservation of the mer geometry of the Ru(III) precursor[37] in the reduced species, which is also supported by DFT calculations (see below).

$$[Ru^{III}(CO)(bpy)Cl_3] + e^- \rightarrow [Ru^{II}(CO)(bpy)Cl_3]^- \quad (9)$$

The cathodic peak at $E_{p,c}$ = −1.99 V observed in the CV of *mer*-[Ru(CO)(bpy)Cl_3]$^-$ in PrCN corresponds formally to an overall three-electron irreversible process (Figure 4, solid curve) that may also involve mer-to-fac isomerization of the one-electron-reduced intermediate complex *mer*-[Ru(CO)(bpy$^{\bullet-}$)Cl_3]$^{2-}$ (see the DFT section). The consumption of three electrons (eq 10), roughly estimated from comparison of the CV peak currents, was unambiguously confirmed by potential-controlled coulometry performed at −2.0 V. The redox process at $E_{1/2}$ = −1.84 V recorded after the exhaustive electrolysis (Figure 4, dashed curve) corresponds to reversible oxidation of the [bpy$^{\bullet-}$] ligand in

(41) Hartl, F.; Chardon-Noblat, S. Unpublished results. The true *cis*-(Cl)-[Ru(CO)(PrCN)(bpy)Cl_2] complex in PrCN (ν(CO) at 1967 cm^{-1}) undergoes irreversible reduction at $E_{p,c}$ = −1.80 V, and the resulting polymer [Ru^0(CO)(PrCN)(bpy)]$_n$ (ν(CO) at 1936 cm^{-1}; bulk electrolysis) is reduced at $E_{1/2}$ = −1.84 V (ΔE_p = 120 mV).

(42) Hartl, F. Unpublished results. A similar observation was made for the complex *fac*-[Re(CO)$_3$(PrCN)(bpy)]$^-$ formed by two-electron reduction of parent *fac*-[Re(CO)$_3$(bpy)Cl] in PrCN: the ν(C≡N) band of the anionic product appeared at 2174 cm^{-1}.

(43) For experimental and theoretical support of this assignment obtained for closely related Os(II) complexes, see refs 44 and 45. Similar (M-X)LCT electronic transitions in the electronic absorption spectrum of *mer*-[$RuCl_3$(CO)(bpy)]$^-$ are reported in the DFT section of this work.

(44) Chardon-Noblat, S.; Da Costa, P.; Deronzier, A.; Mahabiersing, T.; Hartl, F. *Eur. J. Inorg. Chem.* **2002**, 2850–2856.

(45) Jakonen, M.; Hirva, P.; Haukka, M.; Chardon-Noblat, S.; Lafolet, F.; Chauvin, J.; Deronzier, A. *Dalton Trans.* **2007**, 3314–3324.

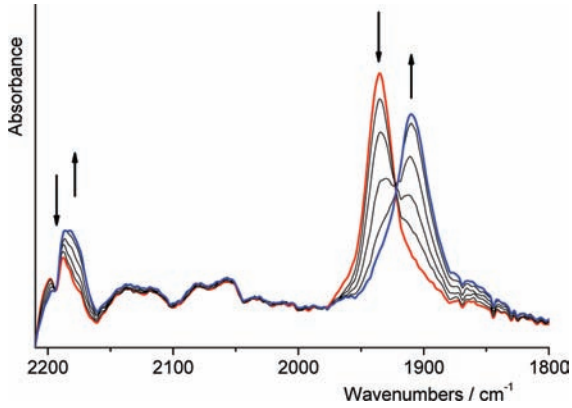

Figure 3. Infrared spectral changes accompanying the reversible bpy-localized 1e$^-$ reduction of $[Ru(CO)(PrCN)(bpy)]_n$ in PrCN/TBAH at T = 293 K, recorded using an OTTLE cell.

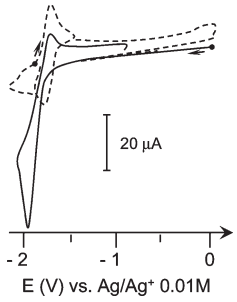

Figure 4. CVs at a vitreous carbon electrode (3 mm diameter). Solid curve: *mer*-$[Ru^{II}(CO)(bpy)Cl_3]^-$ (1.mM in PrCN containing 0.1 M TBAP), initial scan. Dashed curve: $[\{Ru^0(CO)(PrCN)(bpy^{\bullet-})\}^-]_n$ after the exhaustive three-electron reduction of the trichlorido complex at −2.0 V. Scan rate = 100 mV s^{-1}, T = 293 K.

$[\{Ru^0(CO)(PrCN)(bpy^{\bullet-})\}^-]_n$ (eq 6).

$$n[Ru^{II}(CO)(bpy)Cl_3]^- + 3ne^- + n\text{PrCN} \rightarrow [\{Ru^0(CO)(PrCN)(bpy^{\bullet-})\}^-]_n + 3nCl^- \quad (10)$$

The reductive path of *mer*-$[Ru(CO)(bpy)Cl_3]^-$ thus involves rapid dissociation of all three chloride ligands. The small peak observable on the reverse anodic scan at $E_{p,a}$ = −1.75 V (Figure 4, solid curve) thus belongs to the oxidation of the bpy-reduced polymer $[\{Ru(CO)(PrCN)(bpy^{\bullet-})\}^-]_n$ (eq 10), in agreement with the results described above. Merely partial chemical reversibility of the initial bpy-localized one-electron reduction of *mer*-$[Ru(CO)(bpy)Cl_3]^-$ was achieved at T = 213 K in the presence of 0.3 M TEACl instead of TBAP (eq 11). The irreversible behavior is consistent with the facile dissociation of the first Cl^- ligand from the radical trichlorido complex, $[Ru^{II}(CO)(bpy^{\bullet-})Cl_3]^{2-}$ (presumably its fac isomer on grounds of the DFT calculations, see below). For comparison, the less electron-rich radical dichlorido complex $[Ru^{II}(CO)(PrCN)(bpy^{\bullet-})Cl_2]^-$ is stable under identical voltammetric conditions (see above).

$$[Ru^{II}(CO)(bpy)Cl_3]^- + e^- \rightarrow [Ru^{II}(CO)(bpy^{\bullet-})Cl_3]^{2-} \quad (11)$$

It should be noted that the neutral polymer species $[\{Ru^0(CO)(PrCN)(bpy)\}]_n$ can be obtained directly by a carefully controlled bulk electrolysis of *mer*-$[Ru(CO)(bpy)Cl_3]^-$ in PrCN at −1.90 V (eq 12). The PrCN coordination at the Ru(0) centers therefore does not require reduction of the bpy ligands in the polymer (eq 10).

$$n[Ru^{II}(CO)(bpy)Cl_3]^- + 2ne^- + n\text{PrCN} \rightarrow [Ru^0(CO)(PrCN)(bpy)]_n + 3nCl^- \quad (12)$$

Spectroelectrochemistry. The cathodic electrolysis of red-colored *mer*-$[Ru^{III}(CO)(bpy)Cl_3]$ in PrCN was performed at 0 V on a vitreous carbon electrode in a classical electrochemical cell. The one-electron reduction to *mer*-$[Ru^{II}(CO)(bpy)Cl_3]^-$ was monitored in situ by UV/vis spectroscopy, using a 1-mm optical probe. The isosbestic UV/vis spectral changes accompanying the Ru(III)-to-Ru(II) reduction are shown in Figure 5A. The new (Ru−Cl)-to-bpy charge-transfer electronic transitions in the purple product *mer*-$[Ru(CO)(bpy)Cl_3]^-$ manifested as fairly intense visible absorption bands with maxima at 382 and 553 nm have been assigned with the aid of TD-DFT calculations, as described in the DFT section.

In the next, irreversible cathodic step, shown in Figure 5B, *mer*-$[Ru(CO)(bpy)Cl_3]^-$ was carefully reduced at −1.90 V by two electrons (eq 12) to a single orange product absorbing strongly in the visible region at 386 nm and weakly between 500 and 600 nm. These absorption features perfectly match the UV/vis spectrum of the polymer $[Ru(CO)(PrCN)(bpy)]_n$ (see above). Continued electrolysis at −2.0 V then converted the polymer to the one-electron-reduced species $[\{Ru^0(CO)(PrCN)(bpy^{\bullet-})\}^-]_n$ (eq 6). The arising characteristic visible absorption of the $[bpy^{\bullet-}]$ radicals at the ruthenium(0) backbone, having origins in the intraligand $\pi\pi^*$ and $\pi^*\pi^*$ transitions, is shown in Figure 5C. The bulk electrolysis experiment revealed complete solubility of both the polymer $[Ru(CO)(PrCN)(bpy)]_n$ and its bpy-reduced form in PrCN, which is in line with the identical reversible CV responses recorded before (Figure 4, dashed curve) and after the polymer reduction at $E_{1/2}$ = −1.84 V.

The three-step reductive UV/vis spectroelectrochemistry of *mer*-$[Ru^{III}(CO)(bpy)Cl_3]$ in PrCN was repeated also with the OTTLE cell. As expected, the same electronic absorption spectra of the products *mer*-$[Ru^{II}(CO)(bpy)Cl_3]^-$, $[Ru^0(CO)(PrCN)(bpy)]_n$, and $[\{Ru^0(CO)(PrCN)(bpy^{\bullet-})\}^-]_n$ were recorded as depicted in Figure 5A−C. However, in contrast to the cathodic electrolysis of the bulk solution, the reduction of *mer*-$[Ru^{II}(CO)(bpy)Cl_3]^-$ in the thin solution layer led directly to the bpy-reduced polymer $[\{Ru^0(CO)(PrCN)(bpy^{\bullet-})\}^-]_n$ (eq 10), in agreement with the overlapping cathodic waves of the Ru(II) species and the Ru(0) polymer in the conventional cyclic voltammogram (Figure 4). The bpy-neutral polymer $[Ru(CO)(PrCN)(bpy)]_n$ was then obtained by smooth reoxidation at a ca. 150 mV less-negative anodic wave. IR monitoring of the whole cathodic sequence with the aid of the OTTLE cell technique was fully consistent with these assignments. The $\nu(C\equiv O)$ band of *mer*-$[Ru^{III}(CO)(bpy)Cl_3]$ at 2058 cm^{-1} shifted upon the reduction to the corresponding Ru(II) anionic complex down to 1931 cm^{-1}, in

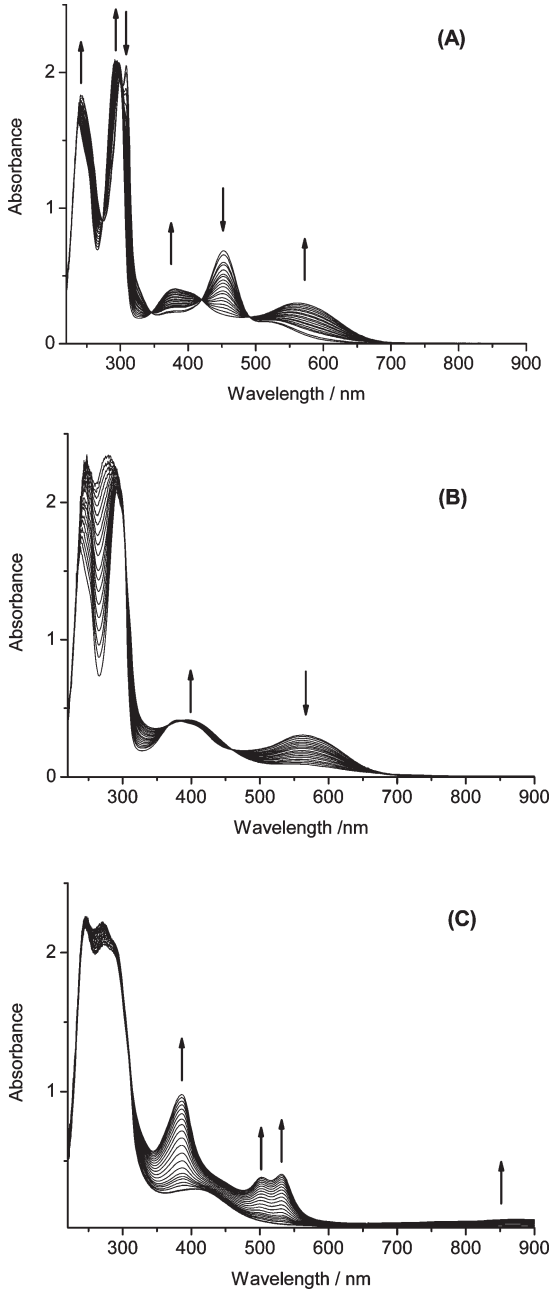

Figure 5. UV/vis spectral changes recorded in the course of three consecutive cathodic processes: (A) *mer*-$[Ru^{III}(CO)(bpy)Cl_3]$ → *mer*-$[Ru^{II}(CO)(bpy)Cl_3]^-$ ($1e^-$); (B) *mer*-$[Ru^{II}(CO)(bpy)Cl_3]^-$ → $[Ru^0(CO)(PrCN)(bpy)]_n$ ($2e^-$); (C) $[Ru^0(CO)(PrCN)(bpy)]_n$ → $[\{Ru^0(CO)(PrCN)(bpy^{\bullet-})\}^-]_n$ ($1e^-$). Conditions: controlled-potential coulometry in PrCN/TBAP at $T = 293$ K, using a bulk electrolysis cell equipped with a 1 mm optical probe (see Experimental Section). Each spectrum corresponds to a 0.1 °C increment.

accordance with the largely metal-localized cathodic step ($\Delta\nu = 127$ cm^{-1}). Subsequent unresolved cathodic conversion of *mer*-$[Ru(CO)(bpy)Cl_3]^-$ to the charged polymer $[\{Ru^0(CO)(PrCN)(bpy^{\bullet-})\}^-]_n$ was accompanied by the simultaneous appearance of new ν(C≡O) and ν(C≡N) absorption bands at 1908 and 2184 cm^{-1}, respectively. The reverse oxidation to $[Ru(CO)(PrCN)(bpy)]_n$ increased these wavenumbers to 1938 and 2194 cm^{-1}, respectively (Figure 6). This process was entirely reversible, as was evidenced by full recovery of $[\{Ru^0(CO)(PrCN)(bpy^{\bullet-})\}^-]_n$ in the

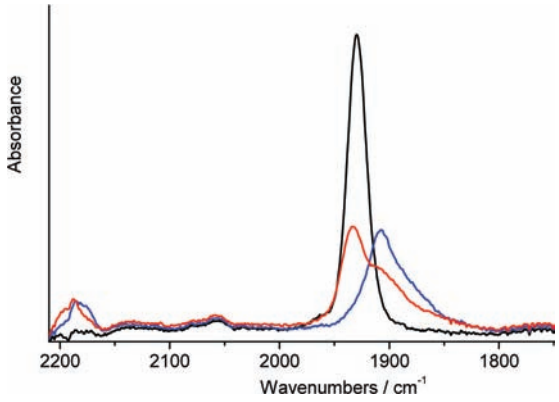

Figure 6. Infrared spectra of the redox series displayed in Figure 5: the starting complex *mer*-$[Ru^{II}(CO)(bpy)Cl_3]^-$ (black line; ν(C≡O) at 1931 cm^{-1}), the polymer $[Ru^0(CO)(PrCN)(bpy)]_n$ (red line; ν(C≡O) at 1938 cm^{-1}), and its bpy-reduced form $[\{Ru^0(CO)(PrCN)(bpy^{\bullet-})\}^-]_n$ (blue line; ν(C≡O) at 1908 cm^{-1}). In the OTTLE cell, the latter reduced species was observed first (eq 10). Its subsequent reoxidation led to $[Ru^0(CO)(PrCN)(bpy)]_n$. Conditions: PrCN/TBAH, $T = 293$ K.

reverse cathodic step. The IR signatures leave no doubts about the assignment, being identical with those depicted above in Figure 3 for this polymer redox couple formed from reduced $[Ru^{II}(CO)(PrCN)(bpy^{\bullet-})Cl_2]^-$ (eqs 6−8).

The combined voltammetric and spectroelectrochemical results clearly prove that the chloride-containing polymer $[\{Ru^0(CO)(bpy)Cl\}^-]_n$ (Chart 1) and its bpy-reduced form cannot be obtained in MeCN or PrCN, in contrast to the uncorroborated assertion in the literature.[15] The chloride substitution by the donor nitrile solvent, induced by the reduction of *mer*-$[Ru^{II}(CO)(bpy)Cl_3]^-$, occurs at room temperature probably already before the formation of the polymer backbone. We therefore attempted to generate $[\{Ru^0(CO)(bpy)Cl\}^-]_n$ in weakly coordinating THF, as described in the next section.

Cathodic Polymerization of *mer*-$[Ru(CO)(bpy)Cl_3]^-$ in THF. Cyclic Voltammetry and Bulk Electrolysis. One-electron oxidation of the Ru(II) center in *mer*-$[Ru(CO)(bpy)Cl_3]^-$ occurs in THF at $E_{1/2} = +0.12$ V as a fully reversible step. In the cathodic region, an irreversible peak was observed at $E_{p,c} = -2.07$ V, followed by a much less intense but reversible redox couple at $E_{1/2} = -2.29$ V ($E_{p,c} = -2.37$ V; Figure 7, cathodic wave (2)). The latter redox process persisted after the exhaustive bulk electrolysis at the first cathodic peak (performed in a drybox under Ar). Addition of PrCN into the THF solution after the exhaustive electrolysis (3:1 THF/PrCN, v/v) led to its partial replacement by a new reversible redox system at $E_{1/2} = -1.90$ V, which can be attributed to the polymer $[Ru(CO)(PrCN)(bpy)]_n$ ($E_{1/2} = -1.84$ V in PrCN, see above, eq 6). The positive shift of the reduction potential agrees with the substitution of the remaining chloride ligand in $[\{Ru^0(CO)(bpy)Cl\}^-]_n$ by a neutral PrCN molecule. Cyclic voltammetry has thus suggested that the chloride-containing polymer $[\{Ru^0(CO)(bpy)Cl\}^-]_n$ (Chart 1) is generated in THF as a stable compound at $E_{p,c} = -2.11$ V, being further reducible at $E_{1/2} = -2.31$ V (eqs 13 and 14 respectively). Monitoring with UV/vis and IR spectroelectrochemistry was employed in the next step to obtain conclusive evidence for this

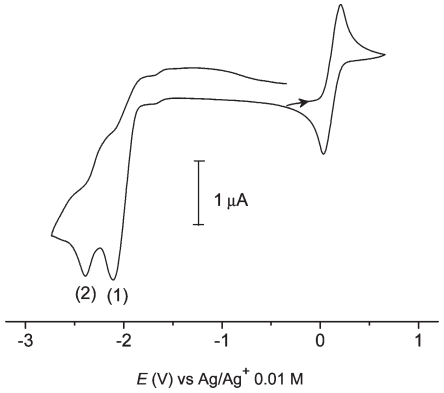

Figure 7. CV of *mer*-$[Ru^{III}(CO)(bpy)Cl_3]$ (3.5 mM) in THF at a Pt disk microelectrode. The cathodic wave (2) belongs to the reversible bpy-localized reduction of $[\{Ru^0(CO)(bpy)Cl\}^-]_n$. Scan rate = 100 mV s^{-1}, T = 293 K.

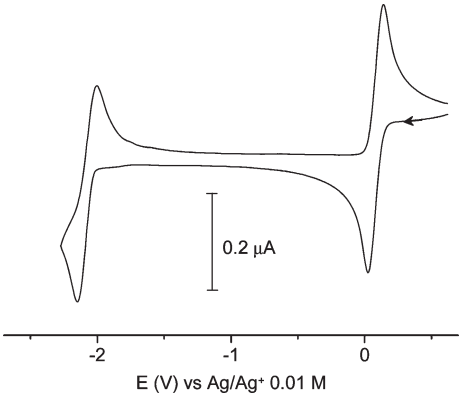

Figure 8. CV of the complex *mer*-$[Ru^{III}(CO)(bpy)Cl_3]$ (3.5 mM) in THF/TBAH at a Pt disk microelectrode. Scan rate = 100 mV s^{-1}, T = 213 K.

path (see below).

$$n[Ru^{II}(CO)(bpy)Cl_3]^- + 2ne^- \rightarrow [\{Ru^0(CO)(bpy)Cl\}^-]_n + 2nCl^- \quad (13)$$

$$[\{Ru^0(CO)(bpy)Cl\}^-]_n + ne^- \rightarrow [\{Ru^0(CO)(bpy^{\bullet-})Cl\}^{2-}]_n \quad (14)$$

At 213 K, the reduction of *mer*-$[Ru^{II}(CO)(bpy)Cl_3]^-$ becomes chemically reversible at $E_{1/2} = -2.10$ V ($I_{p,a}/I_{p,c} = 1$ at $\nu \geq 100$ mV s^{-1}). No polymer reduction was observed (Figure 8). Instead, the resulting radical complex *mer*-$[Ru^{II}(CO)(bpy^{\bullet-})Cl_3]^{2-}$ (eq 11) can be further reduced to the corresponding unstable trianion at $E_{p,c} = -2.92$ V (not studied in detail). This chemically irreversible process is terminated by the formation of the bpy-reduced polymer $[\{Ru^0(CO)(bpy^{\bullet-})Cl\}^{2-}]_n$ (eqs 14, 15, and 16), which could be identified by its anodic wave at $E_{p,a} = -2.38$ V on the reverse potential sweep (cf. Figure 7). For completion, it is important to add that a very similar, almost reversible cathodic response of *mer*-$[Ru^{II}(CO)(bpy)Cl_3]^-$ was recorded also at room temperature when the scan rate was increased to 10 V s^{-1}. The only difference was the cathodic peak of the product $[Ru^{II}(CO)(bpy^{\bullet-})Cl_3]^{2-}$, shifted to $E_{p,c} = -2.78$ V.

$$[Ru^{II}(CO)(bpy^{\bullet-})Cl_3]^{2-} + e^- \rightarrow [Ru(CO)(bpy)Cl_3]^{3-} \quad (15)$$

$$n[Ru^{II}(CO)(bpy)Cl_3]^{3-} \rightarrow [\{Ru^0(CO)(bpy)Cl\}^-]_n + 2nCl^- \quad (16)$$

Compared with the facile chloride substitution in PrCN, the cyclic voltammetry in THF revealed a significantly increased stability of the Ru−Cl bonds in the polymer $[\{Ru^0(CO)(bpy)Cl\}^-]_n$ and its bpy-reduced form. The fairly high solubility of the negatively charged polymer chains in THF is remarkable.

It is noteworthy that the bpy-localized reduction of *mer*-$[Ru^{II}(CO)(bpy)Cl_3]^-$ is an electrochemically quasi-reversible process ($\Delta E_p = 200$ mV, see Figure 8), while the Ru(II) oxidation is electrochemically reversible (ΔE_p = 80 mV, identical with the value obtained under identical conditions for the ferrocene standard). As the one-electron-reduced species $[Ru^{II}(CO)_2(bpy^{\bullet-})Cl_3]^{2-}$ is stable at 213 K on the subsecond time scale, a plausible explanation for this behavior is rapid mer-to-fac isomerization of the radical dianionic ccomplex coupled to the electron transfer described by eq 11, which is assumed to occur on the grounds of the DFT calculations (see below).

An interesting feature of the cathodic behavior of *mer*-$[Ru^{II}(CO)(bpy)Cl_3]^-$ was observed at room temperature for its diluted solution in THF. Compared with the cyclic voltammogram depicted in Figure 7, the concentration of the Ru(II) complex was lower by almost 1 order of magnitude (Figure 9). The Ru(III)/Ru(II) couple (eq 9) was found at $E_{1/2} = +0.08$ V. The irreversible bpy-localized reduction of the trichlorido Ru(II) complex (eq 13) manifested itself as a poorly resolved cathodic wave at ca. −2.08 V, strongly overlapping with a new cathodic peak at $E_{p,c} = -2.15$ V. When the concentration of the parent complex was increased three times (1.5 mM), the cathodic peak at −2.15 V became largely diminished, and a new peak appeared at −2.42 V, which can be attributed to the bpy-based reduction of the polymer $[\{Ru^0(CO)(bpy)Cl\}^-]_n$ (Figure 7, eq 14). We assign tentatively the cathodic peak at −2.15 V to reduction of either the dimer $[Ru^I(CO)(bpy)Cl_2]_2^{2-}$ or a lower oligomer (tetramer, octamer) formed as intermediates along the cathodic polymerization path of *mer*-$[Ru^{II}(CO)(bpy)Cl_3]^-$ (eqs 17 and 18), in analogy with the thoroughly investigated[12] polymerization of the related complex $[Ru^{II}(CO)_2(bpy)Cl_2]$. The reductive polymerization seems to proceed less efficiently at low concentrations of the parent Ru(II) trichlorido complex, which enables the detection of the shorter-chain intermediates on the CV time scale. IR spectroscopic evidence for this assignment is given in the spectroelectrochemical section.

$$2[Ru^{II}(CO)_2(bpy^{\bullet-})Cl_3]^{2-} \rightarrow [Ru^I(CO)_2(bpy)Cl_2]_2^{2-} + 2Cl^- \quad (17)$$

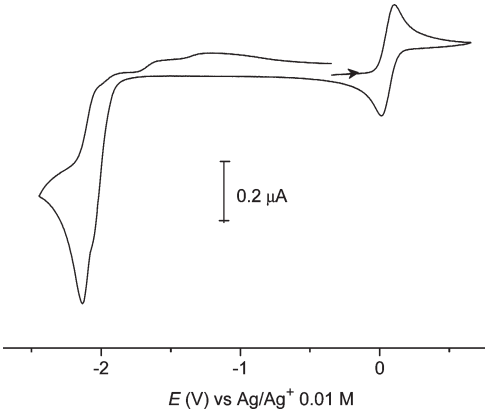

Figure 9. CV of the complex *mer*-[$Ru^{III}(CO)(bpy)Cl_3$] (0.5 mM) in THF/TBAH at a Pt disk microelectrode. Scan rate = 100 mV s^{-1}, T = 293 K. The cathodic wave of $[\{Ru^0(CO)(bpy)Cl\}^-]_n$ (see Figure 7) is absent under these experimental conditions.

$$2[Ru^{I}(CO)_2(bpy)Cl_2]_2^{2-} + 2e^- \rightarrow [\{Ru^{I}(CO)_2(bpy)Cl_2\}_2\{\mu\text{-}Ru^0(CO)_2(bpy)Cl\}_2]^{4-} + 2Cl^- \quad (18)$$

Spectroelectrochemistry. As in PrCN, the initial cathodic step in the IR spectroelectrochemical investigation of the redox series in THF at room temperature was a smooth conversion of *mer*-[$Ru^{III}(CO)(bpy)Cl_3$] (ν(C≡O) at 2054 cm^{-1}) to [$Ru^{II}(CO)(bpy)Cl_3]^-$ (ν(C≡O) at 1933 cm^{-1}; not shown). Further reduction of the Ru(II) precursor of the polymer species, observed in the thin-layer CV ca. 2 V more negatively, resulted in the appearance of a broad ν(C≡O) band of medium intensity at 1873 cm^{-1} (Figure 10). Consistent with the conventional CV (Figure 7), the subsequent cathodic process was localized only ca. 250−300 mV more negatively and yielded a single monocarbonyl product absorbing at 1845 cm^{-1}. The shift of the ν(C≡O) maximum to lower wavenumbers by 28 cm^{-1} is in accordance with the bpy-localized reduction in the Ru(0) polymer (eq 14). A very similar shift of 30 cm^{-1} was recorded for the bpy-localized polymer redox couple $[\{Ru^0(CO)(PrCN)(bpy)\}^m]_n$ (m = 0, −1; eq 6; see Figure 6). The markedly smaller CO-stretching wavenumbers of the polymer products generated in THF ($\Delta\nu$ = −65 and −68 cm^{-1}, respectively) reveal coordination of the chloride ligand at the electron-rich Ru(0) center. Due to the strong (Cl)Ru-to-CO π-back-donation, the negative charge in the polymer redox couple, $[\{Ru^0(CO)(bpy)Cl\}^m]_n$ (m = −1, −2), is probably localized also on the single CO ligand, which is reflected in the large ν(C≡O) band width (Figure 10).[47] As expected, no absorption was observed for the chloride-containing polymers between 2200 and 2150 cm^{-1} where the ν(C≡N) signature of the PrCN ligand in $[\{Ru^0(CO)(PrCN)(bpy)\}^m]_n$ (m = 0, −1) typically occurs (see Figures 2, 3, and 6).

(47) For the same reason, a similar band broadening was observed, for example, in the case of formally Ru(0) complexes $[Ru(CO)_2(NN)(Me)]^-$ (NN = bpy and *N*,*N*′-di-isopropyl-1,4-diazabuta-1,3-diene (iPr-DAB), see Figures 5 and 6 in: Hartl, F.; Aarnts, M. P.; Nieuwenhuis, H. A.; van Slageren, J. *Coord. Chem. Rev.* **2002**, *230*, 107–125.

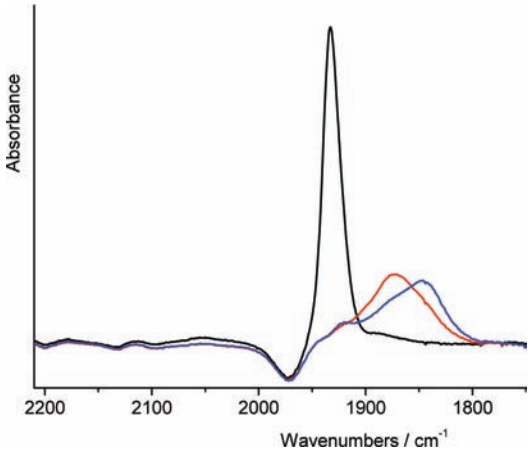

Figure 10. Infrared spectra of the consecutive members of the redox series *mer*-$[Ru^{II}(CO)(bpy)Cl_3]^-$ (black line; ν(C≡O) at 1933 cm^{-1}) → $[\{Ru^0(CO)(bpy)Cl\}^-]_n$ (red line; ν(C≡O) at 1873 cm^{-1}) → $[\{Ru^0(CO)(bpy^{\bullet-})Cl\}^{2-}]_n$ (blue line; ν(C≡O) at 1845 cm^{-1}). Conditions: THF, T = 293 K, an OTTLE cell. The negative reference absorbance at 1968 cm^{-1} corresponds to the THF solvent.

Aimed at the description of the mechanism of the reductive polymerization of $[Ru^{II}(CO)(bpy)Cl_3]^-$, it is important to note that the conversion of the parent complex to the polymer $[\{Ru^0(CO)(bpy)Cl\}^-]_n$ was accompanied by an appearance of intermediate species absorbing in the IR spectrum at 1905 and 1890 cm^{-1} (not shown in Figure 10). We assign these transient ν(C≡O) bands tentatively to di- or oligomeric intermediates formed along the polymerization path, in accordance with the cyclic voltammetric information (Figure 9) and eqs 17 and 18. For a more thorough discussion, it will be necessary to prepare and characterize these oligonuclear complexes separately, similar to the polymerization of $[Ru^{II}(CO)_2(bpy)Cl_2]$.[12]

Useful information about the negatively charged polymers $[\{Ru^0(CO)(bpy)Cl\}^m]_n$ (m = −1, −2) was also obtained from UV/vis spectroelectrochemistry run in parallel with the IR OTTLE experiment. The ultimate reduction product $[\{Ru^0(CO)(bpy^{\bullet-})Cl\}^{2-}]_n$ exhibits a UV/vis spectrum very similar to that of $[\{Ru^0(CO)(PrCN)(bpy^{\bullet-})\}^-]_n$ depicted in Figure 5C. The intraligand absorption maxima of the [$bpy^{\bullet-}$] ligands in the chloride-containing chain are found, however, at slightly different wavelengths, namely, 362 nm ($\pi\pi$*) and 515/548 nm ($\pi^*\pi^*$); the weak $\pi^*\pi^*$ absorption below 800 nm was also observed. On the other hand, the electronic absorption spectrum of $[\{Ru^0(CO)(bpy)Cl\}^-]_n$ does not resemble very much that of $[Ru^0(CO)(PrCN)(bpy)]_n$ (Figure 5B/C). In particular, the chloride-containing polymer shows in the visible region a poorly resolved absorption rising between 900 and 400 nm (see Figure SI1 in Supporting Information), while the PrCN-containing polymer does not absorb below 600 nm. This difference in absorption is tentatively assigned to new low-lying electronic transitions in $[\{Ru^0(CO)(bpy)Cl\}^-]_n$, having a Cl(Ru)-to-bpy charge-transfer character. Note that both ligands in the polymer probably lie in the same (equatorial) plane.

In order to provide direct proof of the chloride coordination at the polymer backbone, we decided to reduce the

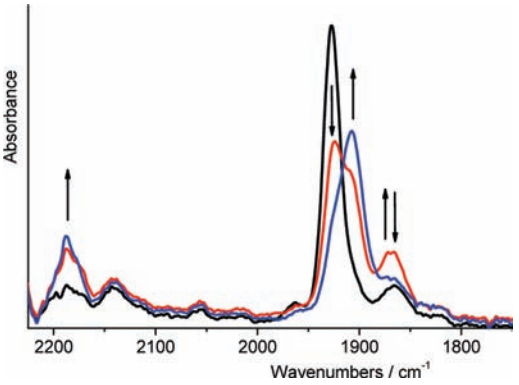

Figure 11. Infrared spectral changes accompanying the two-electron cathodic transformation of *mer*-$[RuCl_3(CO)(bpy)]^-$ (↓) to the transient polymer $[\{Ru^0(CO)(bpy)Cl\}^-]_n$ (↑↓) that further converted to stable $[\{Ru^0(CO)(PrCN)(bpy^{\bullet-})\}^-]_n$ (↑). Conditions: PrCN, T = 193 K, a cryostated OTTLE cell.

precursor *mer*-$[Ru^{II}(CO)(bpy)Cl_3]^-$ in PrCN at 198 K in the presence of the 3×10^{-1} M Et_4NCl electrolyte and monitored this process in situ with IR spectroscopy. As shown in Figure 11, the disappearance of the starting Ru(II) complex (ν(C≡O) at 1928 cm^{-1}) gives first rise to the ν(C≡O) band at 1867 cm^{-1} that belongs to $[\{Ru^0(CO)(bpy)Cl\}^-]_n$, observed at room temperature only in THF. The subsequent substitution of Cl^- by PrCN has been witnessed through gradual disappearance of the ν(C≡O) band at 1867 cm^{-1} and the rise of absorption bands at 2185 and 1907 cm^{-1} due to the ν(C≡N) and ν(C≡O) modes, respectively, of the stable polymer $[\{Ru^0(CO)(PrCN)(bpy^{\bullet-})\}^-]_n$. The PrCN-substituted polymer is generated directly in its bpy-reduced form as dictated by the negative reduction potential of the parent complex *mer*-$[Ru^{II}(CO)(bpy)Cl_3]^-$ (see Figure 6 and the corresponding description in the main text). The chloride substitution reaction of the polymer $[\{Ru^0(CO)(bpy)Cl\}^-]_n$ becomes hindered significantly by the presence of an excess of Cl^-, in line with the reference IR OTTLE experiment performed at 198 K when using TBAH as the supporting electrolyte. In the latter case, the observable amount of $[\{Ru^0(CO)(bpy)Cl\}^-]_n$ was very small, although not completely negligible, as was the case at room temperature, and the ν(C≡N) band signaling that the PrCN coordination was observable from the very first moment of the cathodic electrolysis.

DFT Calculations of *mer*-$[Ru^{II}(CO)(bpy)Cl_3]^-$. The density functional theory calculations[28] focused on the electronic structure and low-energy electronic transitions of the Ru(II) complex *mer*-$[Ru(CO)(bpy)Cl_3]^-$. The study also included the comparison of its energy with that of the hypothetical fac isomer in both the bpy-neutral and one-electron-reduced states and was aimed at understanding the cathodic electropolymerization of *mer*-$[Ru(CO)(bpy)Cl_3]^-$, shown by cyclic voltammetry to be triggered by the one-electron reduction of the bpy ligand,

DFT calculations were run using the ADF program[29] (see the Experimental Section). The isomer *mer*-$[RuCl_3(CO)(bpy)]^-$ was found to be more stable than the hypothetical fac isomer by ~4 kcal mol^{-1}, but the facial isomer of the $1e^-$-reduced complex became preferred by ~12 kcal mol^{-1}. More reliable calculations taking into account the solvent (THF, COSMO model) indicated

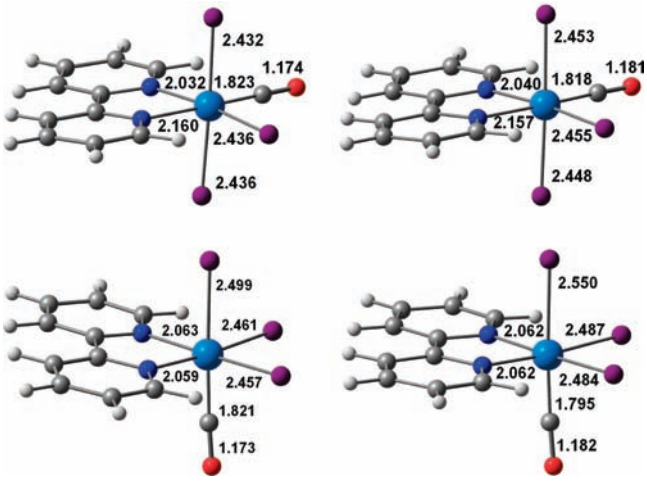

Figure 12. Optimized geometries of the isomeric Ru(II) complexes *mer*-$[RuCl_3(CO)(bpy)]^-$ (left, top) and *fac*-$[RuCl_3(CO)(bpy)]^-$ (left, bottom) and the corresponding bpy-reduced radical species $[Ru^{II}(CO)(bpy^{\bullet-})Cl_3]^{2-}$ (right).

that the two isomers of $[RuCl_3(CO)(bpy)]^-$ had the same energy and the energy difference between their bpy-reduced forms dropped to 2.8 kcal mol^{-1}. The optimized geometries are shown with some relevant distances (ångstroms) in Figure 12. Upon reduction, all of the Ru−Cl bonds in both isomers lengthen slightly. The most pronounced elongation (0.05 Å) was observed for the axial Ru−Cl bond in *fac*-$[RuCl_3(CO)(bpy)]^{2-}$. Changes in the M−C and M−N bond lengths are negligible. The central C−C bond of the bpy ligand gets shorter, reflecting the population of the predominantly π*(bpy) lowest unoccupied molecular orbital (see Figures 12 and 13). Since distances are not always reliable indicators of bond strength, Mayer indices (MI)[38] were calculated. The MI for the Ru−Cl bonds drops from a range of 0.547−0.564 in the mer isomer or 0.488−0.549 in the fac isomer to 0.118−0.123 and 0.097−0.120, respectively, in the reduced complexes. Therefore, dissociation of a chlorido ligand appears a likely process to occur, either in the mer or in the fac isomer, if isomerization takes place, giving rise to a square-pyramidal intermediate with a half-occupied orbital directed toward the empty coordination position. The latter intermediate easily dimerizes, triggering the subsequent oligo- and polymerization process.

TD-DFT calculations were carried out for all species shown in Figure 12, but only the results concerning stable *mer*-$[RuCl_3(CO)(bpy)]^-$ will be discussed. The calculated electronic absorption spectrum of this complex (Figure 13; only the strongest transitions shown) reproduced qualitatively well the recorded experimental spectrum in the visible region (Figure 5A). The general shift of the computed transition energies to lower values compared to the experiment is frequently encountered for electronic transitions having a charge-transfer character. The asymmetric absorption maximum at 382 nm (in PrCN) probably corresponds to the calculated transitions **3**, **4**, and **5** having mixed (M−X)LCT and XLCT characters, respectively. The most intense transition **3** has also a π*(Ru−Cl) → σ*(Ru−Cl) component. The lowest-energy absorption band at 553 nm is attributed to the (M−X)LCT electronic transition **1** that is typical for this

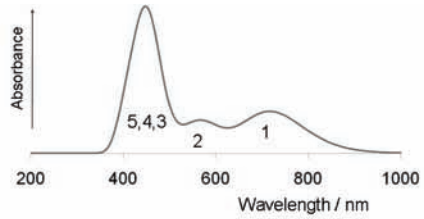

Nr	λ /nm	E /eV	O.S.	Composition
1	719.2	1.72	0.018	H → L (91%)
2	570.9	2.17	0.013	H-1 → L (92%)
3	456.2	2.72	0.046	H → L+2 (49%)
				H → L+3 (28%)
4	425.7	2.91	0.016	H-1 → L+1 (87%)
5	418.2	2.96	0.009	H-3 → L (96%)

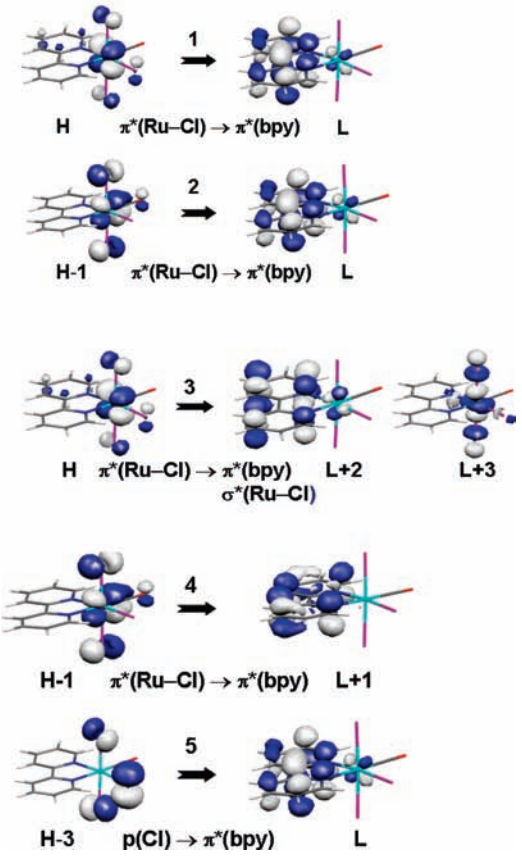

Figure 13. The calculated electronic absorption spectrum of *mer*-[Ru^{II}-(CO)(bpy)Cl_3]$^-$ in the visible region and analysis of the corresponding charger-transfer electronic transitions. The experimental spectrum is depicted in Figure 5A (the product spectrum).

class of complexes. The weak (M−X)LCT electronic transition **2** is not resolved in the experimental spectrum without band deconvolution.

DFT Calculations of *cis*-(Cl)-[Ru^{II}(CO)(MeCN)-(bpy)Cl_2]. This complex may formally exist as three isomers, with axial ligand combinations MeCN/CO (**A**), Cl/MeCN (**B**), and Cl/CO (**C**). DFT calculations have shown that the potential energies of structures **B** and **C** are almost identical ($\Delta E = 1.6$ kcal mol^{-1}). Structure **B** is known from the literature[16] and was therefore selected for the theoretical study aimed at analysis of electronic transitions in the visible and UV regions. The optimized geometry of *cis*-(Cl)-[Ru^{II}(CO)(MeCN)(bpy)Cl_2] (**B**) is depicted with some relevant bond lengths (Å) in Figure SI2 (Supporting Information), showing good agreement with the published crystallographic parameters.

The results of TD-DFT calculations of *cis*-(Cl)-[Ru^{II}-(CO)(MeCN)(bpy)Cl_2] (**B**) are summarized in Figure SI3 (Supporting Information). Good agreement was achieved between the experimental and calculated electronic absorption spectra. Similar to *mer*-[Ru(CO)(bpy)Cl_3]$^-$ (see above), the UV/vis (300−600 nm) absorption of *cis*-(Cl)-[Ru^{II}(CO)-(MeCN)(bpy)Cl_2] (**B**) is dominated by several π^*(Ru−Cl) → π^*(bpy) (at lowest energy) and π(Ru−Cl) → π^*(bpy) charge transfers, that is, (M−X)LCT transitions. Some minor involvement of the equatorial carbonyl ligand exists in the (near) UV excitations.

For the electrochemical analysis, it is important to mention that the reduction of *cis*-(Cl)-[Ru^{II}(CO)-(MeCN)(bpy)Cl_2] (**B**) initially resides, as expected, almost exclusively on the bpy ligand and not on the Ru(II) center. The electrochemical oxidation to the Ru(III) complex, on the other hand, strengthens both axial and equatorial Ru−Cl bonds, in agreement with its reversible nature. The same conclusion can be drawn also for *mer*-[Ru(CO)-(bpy)Cl_3]$^-$ (see above).

Conclusions

The UV/vis and IR spectroelectrochemical experiments combined with cyclic voltammetry and exhaustive electrolysis/coulometry showed that the soluble electron-rich polymer [{Ru^0(CO)(bpy)Cl}$^-$]$_n$ can indeed be obtained from reduced *mer*-[$Ru^{II}Cl_3$(CO)(bpy)]$^-$ as anticipated in the literature,[15] but only in weakly coordinating THF. In contrast, the chloride substitution reaction with a donor solvent is facile in PrCN, where the polymer [Ru(CO)(PrCN)(bpy)]$_n$ is formed. The latter polymer can be also obtained directly by two-electron reduction of *cis*-(Cl)-[Ru(CO)(MeCN)(bpy)-Cl_2] in PrCN, while the derivative [Ru(CO)(MeCN)(bpy)]$_n$ can be prepared in this way from *cis*-(Cl)-[Ru(CO)(MeCN)-(bpy)Cl_2] in THF. In the latter case, the chloride-free product could be distinguished by its reversible bpy-based reduction at $E_{1/2} = -1.90$ V. Other important points are the stability and solubility of the corresponding bpy-reduced polymer form [{Ru^0(CO)(MeCN)(bpy$^{\bullet-}$)}$^-$]$_n$, which was shown to trigger the electrocatalytic reduction of carbon dioxide. The polymer [Ru$(CO)_2$(bpy)]$_n$, the well-known and thoroughly characterized efficient electrocatalyst of carbon dioxide reduction, is poorly soluble in all common polar solvents and needs to be synthesized directly on the catalyst support materials. In this respect, the high solubility of [Ru-(CO)(PrCN)(bpy)]$_n$ and its bpy-reduced form in PrCN is highly remarkable, representing an important achievement in the development and characterization of soluble and hence transportable polymeric materials based on nonbridged metal−metal bonds. A similar difference in solubility was recently reported for the couple [Os$(CO)_2$(bpy)]$_n$ and [Os(CO)(MeCN)(bpy)]$_n$.[19] The mononuclear Os(II) precursors of these polymers are much better suited for mechanistic studies of the cathodic electropolymerization path than the corresponding but more reactive Ru(II) complexes with weaker metal−Cl bonds. This study will therefore be continued with electrochemical reduction of the novel complex *mer*-[$Os^{II}Cl_3$(CO)(bpy)]$^-$, with accent on the mechanism of formation of the soluble

polymeric chain and the chloride substitution in PrCN, as well as on understanding of the apparent strong influence of the carbonyl substitution on the solubility of the ultimate polymeric products.

Acknowledgment. This study was undertaken as a part of the COST Action D29 (project no. D29/0012/04). For financial support, M.H. is grateful to the Academy of Finland (Project No. 115985); F.H. to the Joseph Fourier University in Grenoble (visiting professor in September 2008); and M.J.C. to FCT, POCI, and FEDER (project POCI/QUI/58925/2004).

Supporting Information Available: (a) UV−vis spectroelectrochemistry of *mer*-$[Ru^{II}Cl_3(CO)(bpy)]^-$: reduction in THF (Figure SI1). (b) DFT-optimized structure of the *cis*-(Cl)-$[Ru^{II}(bpy)(CO)(MeCN)Cl_2]$ (Figure SI2). (c) DFT-computed charge-transfer electronic transitions in *cis*-(Cl)-$[Ru^{II}(CO(MeCN))(bpy)Cl_2]$ (Figure SI3). This material is available free of charge via the Internet at http://pubs.acs.org.